bioRxiv preprint doi: https://doi.org/10.1101/346841; this version posted June 14, 2018. The copyright holder for this preprint (which was not certified by peer review) is the author/funder. All rights reserved. No reuse allowed without permission.

A circuit motif in the songbird basal ganglia for computing predicted performance quality

Ruidong Chen*, Pavel A. Puzerey*, Andrea C. Roeser, Tori Riccelli, Archana Podury, Kamal Maher, Alexander Farhang, Jesse H. Goldberg

Department of Neurobiology and Behavior, Cornell University, Ithaca, NY 14853

*Equal contribution

Correspondence:
Jesse H. Goldberg
Department of Neurobiology and Behavior
W121 Mudd Hall
Cornell University
Ithaca, NY 14853

Abstract:	177 words
Main text:	1296 words
Main Figures:	5
Extended Data Figures:	10

bioRxiv preprint doi: https://doi.org/10.1101/346841; this version posted June 14, 2018. The copyright holder for this preprint (which was not certified by peer review) is the author/funder. All rights reserved. No reuse allowed without permission.

Ventral tegmental area (VTA) dopamine neurons contribute to reinforcement learning by signaling prediction error, the difference between actual and predicted outcome[1], but it remains unclear how error is computed[2]. Here we identify in songbirds that a VTA-projecting ventral basal ganglia (vBG) region outside the classic song system[3] is required for song learning and sends prediction error signals to VTA. vBG neurons, including identified VTA-projectors, recorded during singing heterogeneously encoded song timing, predicted error, actual auditory error, and the difference between the two (prediction error). Viral tracing revealed novel inputs to vBG from auditory and vocal motor thalamus, auditory and vocal motor cortex, and VTA. Our findings reveal a classic actor-critic circuit motif[4-6], previously unrecognized in the songbird BG, in which a ventral critic learns the 'prediction' component of a prediction error signal that is relayed by dopaminergic midbrain to a dorsal actor (the vocal motor BG nucleus Area X). Thus a circuit motif with established utility in foraging for reward in mammals is ancestral and can be repurposed for computing predicted performance error during motor sequence learning.

When practicing a piano concerto, you could evaluate your performance relative to a fixed target, such as an auditory memory of Chopin's Prelude No. 4. Yet reinforcement learning (RL) theory suggests improved learning if you instead learn from prediction errors, in which a note is reinforced only if it sounds better than predicted based on your past performance[4]. Zebra finches learn to imitate a sequence of song notes, or syllables, acquired from a single tutor, suggesting they have a 'fixed target' they aspire to learn[7]. Yet consistent with RL theory, song syllables are not evaluated against this fixed target but are instead evaluated against syllable-specific performance benchmarks that change with practice[8]. Specifically, Area X projecting dopamine (DA) neurons recorded during singing exhibit error signals, important for song learning[9-11], characterized by phasic suppressions following worse-than-predicted syllable outcomes and activations following better-than-predicted ones (Fig. 1a,b).

To identify upstream pathways that may drive these signals, we injected retrograde tracer into the Area X-projecting part of VTA (VTAx). Consistent with past work, retrogradely labeled neurons were observed in the ventral intermediate arcopallium (AIV), a high-order auditory cortical region required for song learning[3,12](Extended Data Fig. 1). VTA-projecting AIV neurons (AIVvta) recorded during singing are activated by distorted auditory feedback (DAF)-induced

bioRxiv preprint doi: https://doi.org/10.1101/346841; this version posted June 14, 2018. The copyright holder for this preprint (which was not certified by peer review) is the author/funder. All rights reserved. No reuse allowed without permission.

error[12], at the same time that VTAx neurons are suppressed[8]. We thus wondered if AIVvta activation could directly induce suppression in VTAx firing. We recorded VTA neurons in anesthetized birds as we electrically stimulated AIV (Fig. 1c). AIV stimulation induced phasic suppressions in wide spiking, antidromically identified VTAx neurons and bursts in thin-spiking VTA interneurons that could inhibit VTAx activity (Fig. 1d-e). Thus VTA contains a local inhibitory circuit that can invert excitatory signals from AIV (Fig. 1i), consistent with the idea that performance error-induced activations in AIV can drive pauses in VTAx firing during singing.

Following tracer injection into VTAx, retrogradely labeled neurons were also observed in the ventral pallidum and overlying ventromedial striatum (Extended Data Fig. 2), as previously reported[3,13]. Because striatal and pallidal cell types can be spatially intermingled in birds[14] we term this region ventral basal ganglia (vBG). To test its role in song learning, we performed sham or real excitotoxic vBG lesions in juvenile birds and evaluated their adult song (Methods). vBG lesions significantly impaired song learning (Extended Data Fig. 3).

Learning deficits following vBG lesion suggest a role in song evaluation. To test how vBG may guide learning, we recorded vBG neurons in singing birds while controlling perceived error with distorted auditory feedback (DAF, see Methods)(Fig. 1b)[15,16]. Beginning days prior to recordings, a specific 'target' song syllable was either distorted with DAF or, on randomly interleaved renditions, left undistorted altogether (distortion rate 48.0±1.4%, mean ± s.e.m., n=38 birds). Previous studies showed that syllable-targeted DAF, though not generally aversive[17], induces a perceived error on distorted renditions such that undistorted renditions are reinforced[15,16]. Over days, DAF also reduces the predicted quality specifically of the target syllable such that undistorted renditions are signaled by VTAx DA neurons as better-than-predicted[8] (Fig 1a).

Significant auditory error responses were observed in 29/122 vBG cells (Fig. 2, Methods). We defined responses as error-activated (n=14) or error-suppressed (n=15)(Methods). Some error-suppressed neurons exhibited significant phasic activations immediately following undistorted renditions of the target syllable, analogous to the positive prediction error signal previously observed in VTAx neurons (n=6, Fig. 2b, Methods). Latencies and durations of error responses were commensurate with those observed in downstream VTAx DA neurons (Extended Data Fig. 4). Analysis of movement patterns with microdrive-mounted accelerometers demonstrated that error responses were not attributable to body movement (Extended Data Fig. 5). Error responses were rarely observed following passive playback of song to non-singing birds ($p>0.05$ in 13/14

bioRxiv preprint doi: https://doi.org/10.1101/346841; this version posted June 14, 2018. The copyright holder for this preprint (which was not certified by peer review) is the author/funder. All rights reserved. No reuse allowed without permission.

neurons, WRS test), consistent with singing-related performance error (Extended Data Fig. 6a-b). Yet two neurons appeared purely auditory in nature because they exhibited similar song-locked firing patterns during active singing and passive playback (Extended Data Fig. 6 c-d).

Many non-error responsive vBG neurons were distinguished by their temporally precise song-locked firing (Fig. 3 and Extended Data Fig. 7a, n=8/159). One class exhibited ultra-sparse discharge aligned to specific song syllables (Fig. 3a and Extended Data Fig. 7b, n=2). Another class exhibited high frequency bursts aligned to specific song time-steps with millisecond precision (Fig. 3b and Extended Data Fig. 7c, n=6). Other vBG cell types exhibited prominent phasic activations or suppressions immediately prior to the target-time of the song, consistent with predicted error and predicted quality signals, respectively (Fig. 3c, Extended Data Fig. 7d-e, n=10). Yet other neurons were simply gated on or off by song state (Extended Data Fig. 7g-i, n=10) or exhibited no detectable song-locked activity (Extended Data Fig. 7f, n=60). These diverse cell types were spatially intermingled (Extended Data Fig. 8).

Antidromic and collision testing methods were used to identify VTA-projecting vBG (vBGvta) neurons (n=7/100 tested). VTA-projecting neurons with low mean firing rates (<50 Hz) could exhibit significant phasic activation following undistorted targets (Fig. 4c, Methods) or prior to the song target time (Fig. 4d). vBGvta neurons with high mean firing rates (>50 Hz) could exhibit error responses (Fig 4e,g) and pauses in firing immediately prior to the target time-step of the song (Fig. 4f-h).

What inputs to vBG could account for this stunning diversity of singing, auditory error, and error prediction-related firing? Using retrograde and anterograde viral tracing strategies, we identified inputs to vBG from (1) RA, a vocal motor cortex-like nucleus known to send precise motor command signals to brainstem motor neurons[18,19]; (2) Uva, a motor thalamic nucleus known to send precise song timing information to HVC, a premotor cortical nucleus[20,21], (3) DLM, the Area X-recipient thalamic nucleus known to send song modulated signals to premotor cortical nucleus LMAN[22], (4) AIV, an auditory cortical area known to send 'actual' (just-heard) auditory error signals to VTA[12], (5) Ovoidalis, the primary auditory thalamus; and (6) VTAx dopamine neurons, known to send performance prediction error signals to Area X[8] (Extended Data Figs. 9-10).

The reciprocal vBG-VTAx loop is notable because it strongly resembles 'spiraling' pathways that link ventral to dorsal BG through VTA in mammals and which are a cornerstone of

bioRxiv preprint doi: https://doi.org/10.1101/346841; this version posted June 14, 2018. The copyright holder for this preprint (which was not certified by peer review) is the author/funder. All rights reserved. No reuse allowed without permission.

actor/critic models of reward-based decision making (pink lines, Fig 5a,b)[4-6,23]. In these models, a ventral critic implements DA-modulated plasticity to learn a state-dependent value function, for example a time- or cue-dependent reward prediction. This ventral critic projects to VTA and provides DA neurons with the temporally precise 'prediction' component of reward prediction error[24]. VTA projects back to the ventral critic to update predicted state-value as well as to a dorsal actor which implements DA-modulated plasticity to learn state-dependent, reward-maximizing policy[4-6].

Our anatomical results identify a strikingly similar actor/critic architecture, previously unrecognized in the songbird BG, that accounts for many of the vBG neural signals we observed (Fig 5b). Specifically, motor cortical (RA) and thalamic (Uva) inputs provide state representations in the form of 'time-step' in song that could explain the observed vBG timing responses (Fig 3). AIV inputs provide information about 'actual' (just-heard) auditory error[12] and could explain the error responses (Fig 2). VTAx inputs could enable DA-modulated thalamo- or cortico-striatal plasticity[25] of Uva or RA inputs, respectively, to compute a state-dependent value function in the form of song time-step dependent predicted error (Fig 5b). This explains the temporally precise prediction signals, such as the pre-target bursts and pre-target pauses, that can be routed from vBG to VTA (Fig4 d,f-h). Thus, the vBG contains information necessary to signal the difference between predicted and actual error (Fig 2a-b and Fig 4c). As in mammals, VTA DA prediction error signals project to vBG to update state-dependent predictions, as well as to a dorsal BG module (Area X) to update action selection policy[10,11,26].

We thus show that a circuit motif for computing reward prediction during foraging is ancestral and can be repurposed to compute performance prediction error during motor sequence learning.

bioRxiv preprint doi: https://doi.org/10.1101/346841; this version posted June 14, 2018. The copyright holder for this preprint (which was not certified by peer review) is the author/funder. All rights reserved. No reuse allowed without permission.

Figure 1: An auditory cortical projection to VTA suppresses VTAx dopamine neurons through feedforward inhibition.

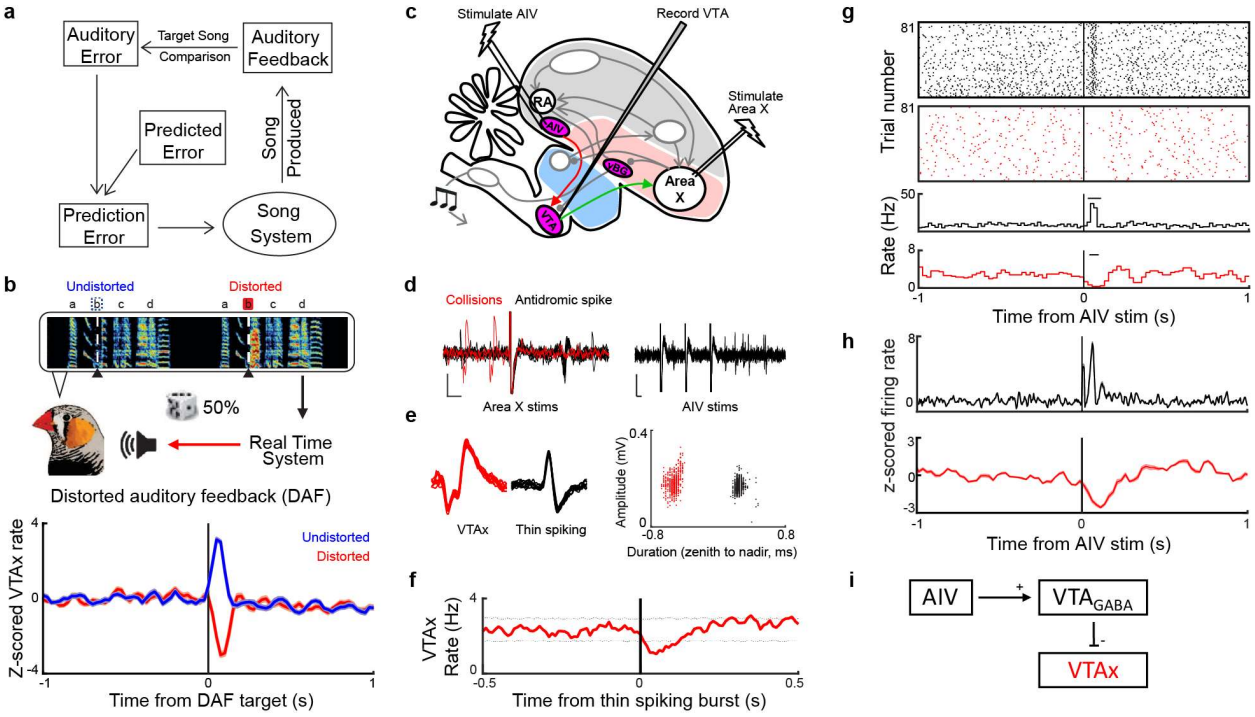

a, Schematic of song production and evaluation system. **b**, Syllable-targeted DAF (top) results in dopaminergic prediction error signals (bottom, from ref[8]). **c**, Test of VTAx response to AIV stimulation. **d-g,** Experiment conducted on simultaneously recorded wide-spiking VTAx neuron and thin-spiking neuron. **d**, Antidromic identification (left), and AIV stimulation (right). **e**, Units in **(d-g)** exhibited distinct waveforms. **f**, Cross-correlogram of spontaneous firing between the two units. Dotted lines, 95% confidence interval (Methods). **g**, Raster plots (top) and rate histograms (bottom) of thin spiking (black) and VTAx neuron (red), aligned to AIV stimulation. Horizontal bars indicate significant response ($p<0.05$, Z test, Methods). **h**, Average Z-scored response to AIV stimulation from 4 VTAx (red) and 7 thin-spiking neurons (black). **i**, Summary: AIV can inhibit VTAx neurons by activating local interneurons.

bioRxiv preprint doi: https://doi.org/10.1101/346841; this version posted June 14, 2018. The copyright holder for this preprint (which was not certified by peer review) is the author/funder. All rights reserved. No reuse allowed without permission.

Figure 2: vBG neurons exhibit error responses during singing

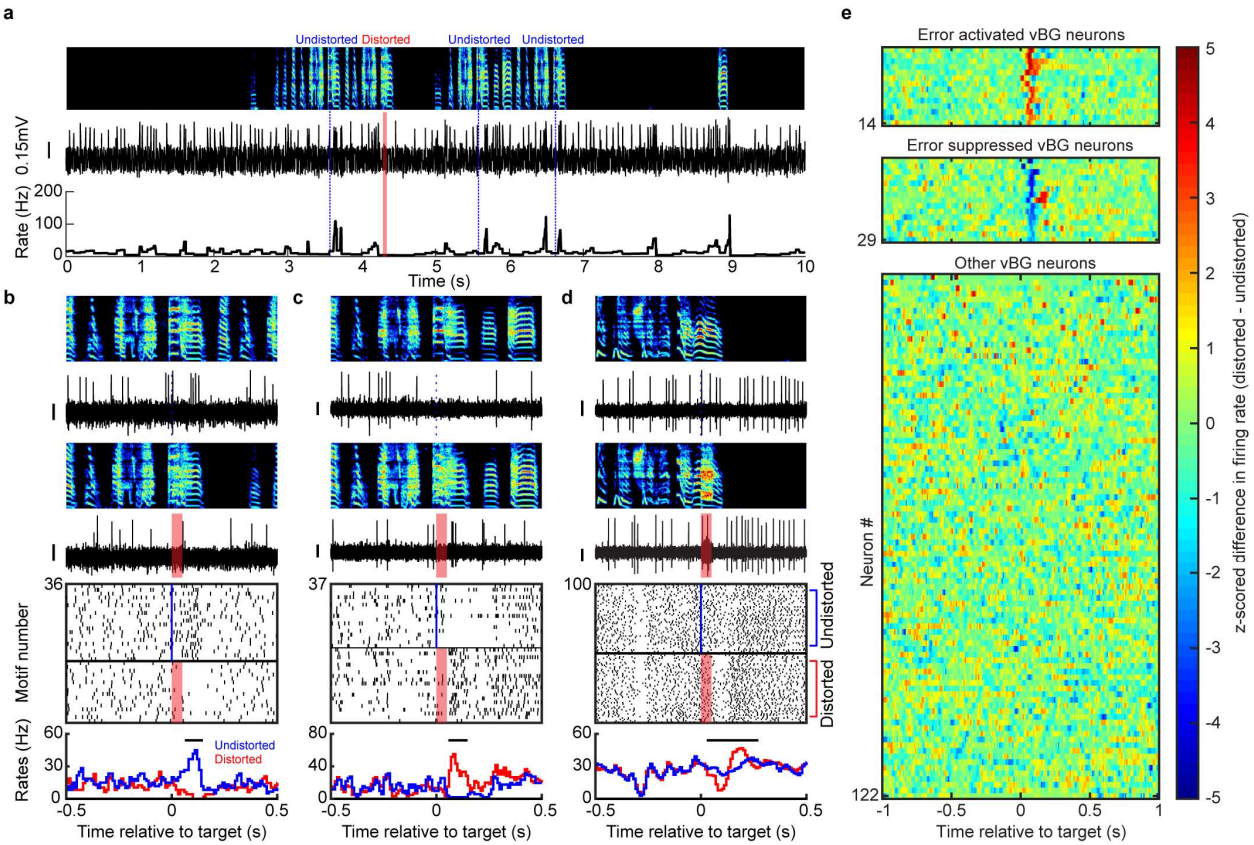

a, Spectrogram (top), discharge (middle) and instantaneous firing rate (bottom) of a vBG neuron recorded during singing. (DAF, red shading; undistorted targets, blue lines). **b**, Expanded view of neuron from (**a**). Top to bottom: spectrograms, spiking activity during undistorted and distorted trials, corresponding spike raster plots and rate histograms (all aligned to target onset). Horizontal bars in histograms indicate significant different response ($P < 0.05$, WRS test, Methods). **c** and **d**, additional examples of error activated and error suppressed neurons, same format as (**b**). **e**, Each row plots the z-scored difference between undistorted and distorted target-aligned rate histograms. Error activated neurons (top, n=14), error suppressed neurons (middle, n=15), and non-error responsive neurons (bottom, n=93) are independently sorted by maximal z-score.

bioRxiv preprint doi: https://doi.org/10.1101/346841; this version posted June 14, 2018. The copyright holder for this preprint (which was not certified by peer review) is the author/funder. All rights reserved. No reuse allowed without permission.

Figure 3: Example vBG neurons that encode precise song timing and pre-target bursts during singing

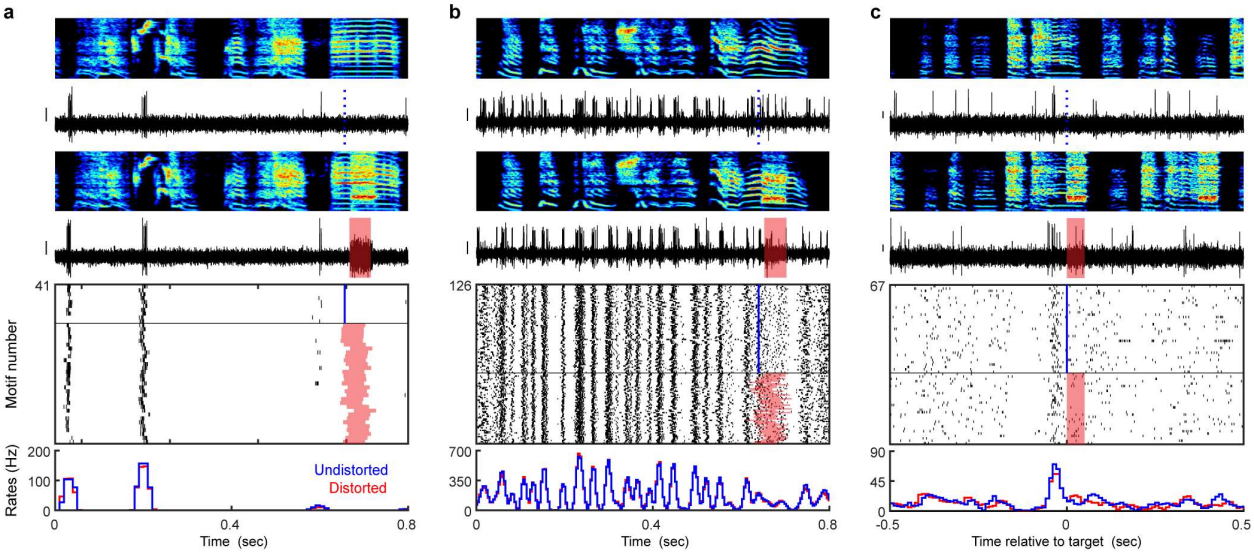

a-c, Top to bottom: spectrograms, spiking activity during undistorted and distorted trials, corresponding spike raster plots and rate histograms for a vBG neuron with sparse, temporally precise discharge (**a**), one with time-locked bursts that tile the song (**b**), and one with a pre-target burst characterized by pronounced activation immediately prior to the targeted time in the song (**c**). Y scale bar for spiking activity is 0.15 mV.

bioRxiv preprint doi: https://doi.org/10.1101/346841; this version posted June 14, 2018. The copyright holder for this preprint (which was not certified by peer review) is the author/funder. All rights reserved. No reuse allowed without permission.

Fig. 4: Antidromically identified VTA-projecting vBG neurons exhibit predicted and actual error responses.

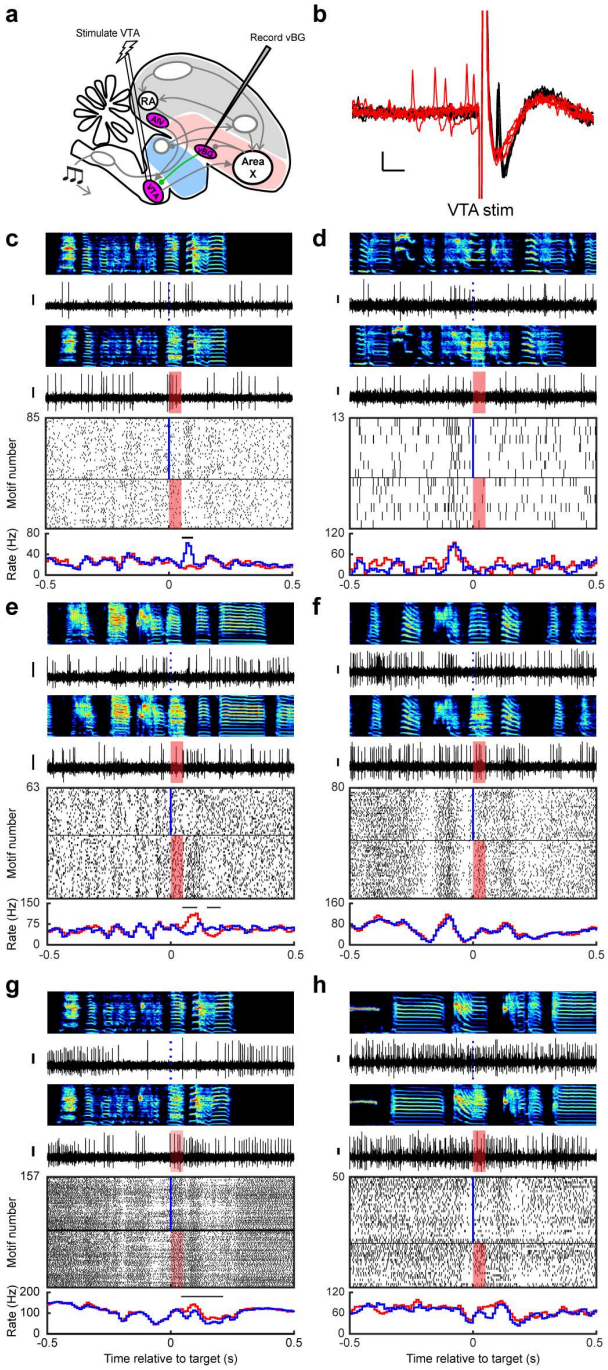

a-b, Stimulation and recording electrodes were chronically implanted into VTA and vBG, respectively, for antidromic identification of VTA-projecting vBG neurons (vBGvta). **b,** Antidromic (black) and collision (red) testing of the neuron shown in panel c. **c-h,** Song-locked firing patterns of six confirmed vBGvta neurons, plotted as in Fig. 3, reveal activity patterns

bioRxiv preprint doi: https://doi.org/10.1101/346841; this version posted June 14, 2018. The copyright holder for this preprint (which was not certified by peer review) is the author/funder. All rights reserved. No reuse allowed without permission.

including activation following undistorted targets (**c**), pre-target bursts (**d**), error-induced activation (**e**), and pre-target pauses (**f-h**).

bioRxiv preprint doi: https://doi.org/10.1101/346841; this version posted June 14, 2018. The copyright holder for this preprint (which was not certified by peer review) is the author/funder. All rights reserved. No reuse allowed without permission.

Figure 5: An actor-critic circuit motif for computing predicted performance quality

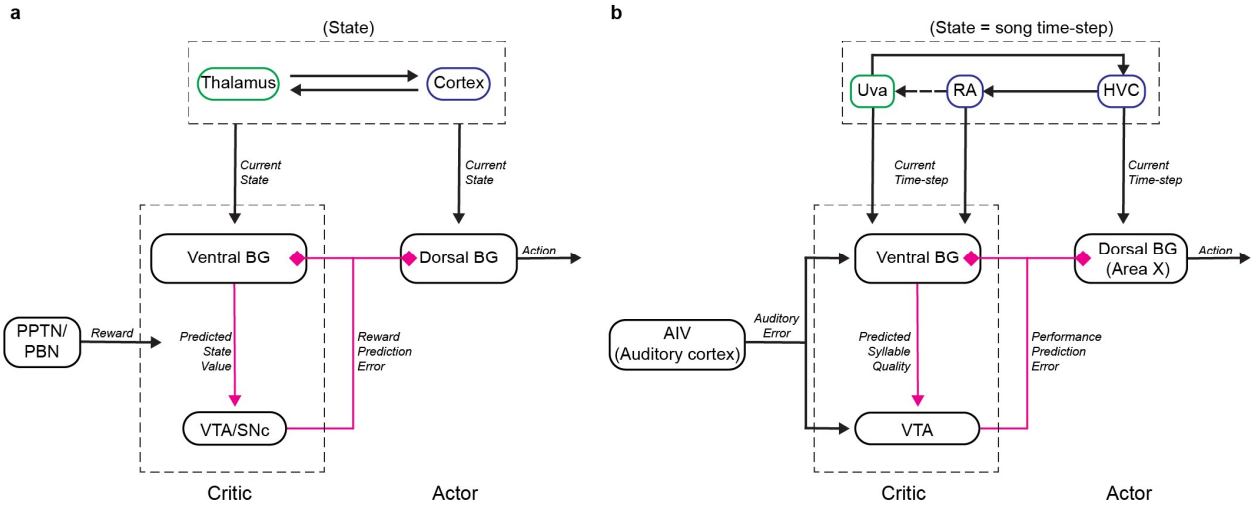

a, Actor-critic circuit motif in mammalian BG inspired by refs[4-6]. **b,** Anatomy and signaling in songbird vBG reveals a similar motif.

bioRxiv preprint doi: https://doi.org/10.1101/346841; this version posted June 14, 2018. The copyright holder for this preprint (which was not certified by peer review) is the author/funder. All rights reserved. No reuse allowed without permission.

Methods

Subjects

Subjects were 61 male zebra finches. Animal care and experiments were carried out in accordance with NIH guidelines and were approved by the Cornell Institutional Animal Care and Use Committee.

Surgery and histology

All surgeries were performed with isoflurane anesthetization. For functional mapping experiments (4 birds, Fig. 1), bipolar stimulation electrodes were implanted into AIV and Area X[8,12]. Briefly, AIV coordinate was determined by its anterior and ventral position to RA, and Area X coordinate was +5.6A, +1.5L relative to lambda and 2.65 ventral relative to pial surface, at a head angle of 20 degrees. Recordings were made in VTA using a carbon fiber electrode (1 MOhm, Kation Scientific). VTA was identified by anatomical landmarks. Specifically, the boundaries of DLM and Ovoidalis were determined by spontaneous firing and auditory responses. Recordings were then made at the same AP position, +0.6L relative to lambda and 6.5 ventral relative to pial surface, at a head angle of 55 degrees. Area X projecting neurons were further confirmed by antidromic response and collision testing. Location of the stimulating electrodes was verified histologically.

For vBG lesion (13 birds, 39-52 dph), a bipolar stimulation electrode was implanted into Area X and the center of vBG was electrophysiologically mapped by finding units suppressed by Area X stimulation. 115nl of 2% N-methyl-DLaspartic acid (NMA; Sigma, St Louis, MO) was injected into vBG bilaterally.

For awake-behaving electrophysiology (38 birds, 87-355 dph), custom made microdrives carrying an accelerometer (Analog Devices AD22301), linear actuator (Faulhaber 0206 series micromotor) and homemade electrode arrays (5 electrodes, 3-5 MOhms, microprobes.com) were implanted into vBG by coordinates (4.4-5.4A, 1.1-1.5L, 3.5V, head angle 20 degrees). In 19/38 birds, a bipolar stimulation electrode was implanted into VTA using anatomical landmarks as described above. After each experiment, small electrolytic lesions (30 μA for 60 s) were made with one of the recording electrodes. Brains were then fixed, cut into 100 μm thick sagittal sections for histological confirmation of stimulation electrode tracks and reference lesions.

bioRxiv preprint doi: https://doi.org/10.1101/346841; this version posted June 14, 2018. The copyright holder for this preprint (which was not certified by peer review) is the author/funder. All rights reserved. No reuse allowed without permission.

For vBG tracing experiments (6 birds), 40nl of self-complementary adeno-associated virus (scAAV9) with CBh promoter carrying GFP was injected into vBG in two coordinates (4.6/4.9A, 1.3L, 4V). Upstream neurons retrogradely infected and expressing GFP could be observed in RA, AIV, Uva, Ov, DLM, and VTA. To determine if vBG share common inputs with HVC, in addition to scAAV9 in vBG, fluorescently labeled cholera toxin subunit B (CTB, Molecular Probes) was injected into HVC. To determine if vBG share common inputs with Area X, CTB was injected into Area X, and brain sections were immuno-stained with antibodies to tyrosine hydroxylase (Millipore AB152, 1:1000).

Functional mapping between AIV and VTA

Neurons were classified as Area X-projecting (VTAx) based on antidromic stimulation and collision testing (200 μs pulses, 100-300 μA). A burst of AIV stimulation consisting three 200 μs pulses with 10ms inter-pulse-interval was delivered every 1.5-2 s, with 300 μA current amplitude. VTA neurons not responsive to Area X stimulation were also tested for AIV stimulation. All VTAx neurons and those putative interneurons activated by AIV stimulation were further analyzed. To determine if VTA neurons respond to AIV stimulations, spiking activity within ±1 second relative to stim burst onset was binned in a moving window of 30 ms with a step size of 5 ms. Each bin within after stim was tested against all the bins in the previous 1 second (the prior) using a z-test. Windows where at least 4 consecutive bins with $p<0.05$ were considered significant. The response onset and offset were required to bracket lowest (for phasic decrease) or highest (for phasic increase) firing rate after stim onset. For the simultaneously recorded putative VTA interneuron (PIN) and VTAx neuron (Fig. 1d-g), we constructed rate histogram of VTAx neuron spiking events aligned to spiking events of PIN with preceding ISI > 10ms. To assess the significance of VTAx rate suppressions following PIN spiking, 1000 surrogate rate histograms were generated by randomly time-shifting each trial of PIN spiking aligned data over the duration of the histogram (2 seconds). Response was considered significant when VTAx firing rate dropped below 5th percentile or exceeded 95th percentile of the surrogate data.

Song imitation score

Song learning in vBG lesioned and control birds was assessed by song similarity between pupil (at 90 dph) and their tutors. We computed imitation scores using an automated procedure

bioRxiv preprint doi: https://doi.org/10.1101/346841; this version posted June 14, 2018. The copyright holder for this preprint (which was not certified by peer review) is the author/funder. All rights reserved. No reuse allowed without permission.

based on Sound Analysis Pro (SAP) algorithm[12,27]. Briefly, the tutor motif was segmented into syllables by hand. Syllables in the pupil song were determined by finding the section of pupil song with highest SAP similarity to each tutor syllable. Additionally, a sequencing score was computed as the similarity of the next syllable in tutor song and the next section in the pupil song. Imitation score was the product of song similarity and sequence similarity[12].

Syllable-targeted distorted auditory feedback

Postoperative birds with microdrive implant were placed in a sound isolation chamber and given at least a day to habituate to distorted auditory feedback (DAF) as described previously[8]. Briefly, ongoing singing was analyzed by Labview software to target specific syllables, and two speakers inside the chamber played a 50ms DAF sound on top of bird's singing on 50% of randomly selected target renditions. DAF was either a broadband sound band passed at 1.5-8 kHz, the same spectral range of zebra finch song, or a segment of one of the bird's own non-target syllables displaced in time.

Passive playback of the bird's own song and DAF

For passive playback of the bird's own song, we played back randomly interleaved renditions of the undistorted and distorted motifs of the bird's own song during awake, non-singing periods. The loudness of playback was adjusted to match the average peak loudness of zebra finch song[8,12].

Analysis of neural activity

Neural signals were band-passed filtered (0.25-15 kHz) in homemade analog circuits and acquired at 40 kHz using custom Matlab software. Single units were identified as VTA-projecting by antidromic identification and antidromic collision testing (Fig 4a,b). Spike sorting was performed offline using custom Matlab software. Instantaneous firing rates (IFR) were defined at each time point as the inverse of the enclosing interspike interval (ISI). Firing rate histograms were constructed with 10 ms bins and smoothed with a 3-bin moving average. All data was acquired during undirected song, except for the neuron in Fig. 4h, which was recorded during female-directed song.

bioRxiv preprint doi: https://doi.org/10.1101/346841; this version posted June 14, 2018. The copyright holder for this preprint (which was not certified by peer review) is the author/funder. All rights reserved. No reuse allowed without permission.

Performance error response. To identify performance-error related neurons, we assessed the difference in firing rate between distorted and undistorted singing renditions as previously described[12,28]. Neurons with less than 10 trials of either distorted or undistorted renditions of the target syllable were excluded from this analysis. Briefly, we performed a WRS test (p=0.05) on the number of spikes in distorted vs. undistorted renditions in 30 ms windows. Windows were shifted in 5 ms steps and considered significant when at least 4 consecutive windows had $p<0.05$. Error-related neurons were classified as error-activated if the firing rate is higher in distorted trials in window of significance, and error suppressed if the firing rate is higher in undistorted trials. For error suppressed neurons, we also performed z-test on the firing rate following undistorted trials with 500ms before target as baseline period. Neurons with significant rate increases following target were identified as prediction error neurons.

To test if error responses were attributable to purely auditory responses to a different sound, we performed the same analysis for distorted and undistorted renditions during passive playback of bird's own song (BOS) playback in 12/24 error neurons. Only one neuron exhibited an error response during passive playback. This neuron also exhibited similar song-locked firing during both singing and listening (Extended Data Fig. 6c). One other error responsive neuron also appeared auditory, although the part of playback that contained target syllable was masked by calls (Extended Data Fig. 6d).

We compared the latency and duration of error response to those of VTAx neurons from a previous dataset[8]. Latency and duration was defined by the onset and onset-offset interval of significant windows in WRS test as described above. Two auditory neurons described above were not included in this analysis.

Song timing related activity. Sparseness index was used to identify putative song-related MSNs. This method has been described elsewhere and separates MSNs from other striatal cell types in the dorsal basal ganglia nucleus Area X[29]. For each neuron, we calculated rate histograms aligned to syllable onset for all syllables. Then we normalized these histograms over all syllables to generate a probability density function p_i over N bins. An entropy-based sparseness index was computed as follows:

$$Sparseness\ Index = 1 + \frac{\sum_{i=1}^{N} p_i \log(p_i)}{\log(N)}$$

bioRxiv preprint doi: https://doi.org/10.1101/346841; this version posted June 14, 2018. The copyright holder for this preprint (which was not certified by peer review) is the author/funder. All rights reserved. No reuse allowed without permission.

Intermotif pairwise correlation coefficient (CC) was used to identify neurons that had highly time-locked firing to song motifs (timing neurons), as previously described[29]. Motif aligned IFR was time warped to the median duration of all motifs, mean-subtracted, and smoothed with a Gaussian kernel of 20ms SD, resulting in $\boldsymbol{r_i}$ for each motif. The Intermotif CC was defined as the mean value of all pairwise CC between $\boldsymbol{r_i}$ as follows:

$$ICC = \frac{1}{N_{pairs}} \sum_{j>i}^{N_{pairs}} CC_{ij}$$

$$CC_{ij} = \frac{\boldsymbol{r_i} \cdot \boldsymbol{r_j}}{\sqrt{\boldsymbol{r_i}^2 \boldsymbol{r_j}^2}}$$

To assess significance of CC distributions, we computed new pairwise CC values for each neuron by adding random, circular time shifts to each spiketrain. CC was considered significant when the real distribution was significantly different from that of randomly shuffled data ($P<0.01$, Kolmogorov-Smirnov test).

Quantification of movement

An accelerometer (Analog Devices AD22301) was mounted on microdrives to quantify gross body movements as described previously[8]. Briefly, movement onsets and offsets were determined by threshold crossings of the band-passed, rectified accelerometer signal. To test if error responses could be explained by a difference in movement rate following DAF, for each bird we calculated onset times of movements relative to song target time. Then we performed a WRS test ($p=0.05$) on the number of movement onsets in distorted vs. undistorted renditions in 30 ms windows. Windows were shifted in 5 ms steps and considered significant when at least 4 consecutive windows had $p<0.05$.

Imaging

Imaging data was acquired with a Leica DM4000 B microscope and a Zeiss LSM 710 Confocal microscope. Image processing was done with ImageJ.

Data Availability

All data are available upon request.

bioRxiv preprint doi: https://doi.org/10.1101/346841; this version posted June 14, 2018. The copyright holder for this preprint (which was not certified by peer review) is the author/funder. All rights reserved. No reuse allowed without permission.

References

1 Schultz, W., Dayan, P. & Montague, P. R. A neural substrate of prediction and reward. *Science* **275**, 1593-1599 (1997).

2 Tian, J. *et al.* Distributed and Mixed Information in Monosynaptic Inputs to Dopamine Neurons. *Neuron* **91**, 1374-1389, doi:10.1016/j.neuron.2016.08.018 (2016).

3 Gale, S. D., Person, A. L. & Perkel, D. J. A novel basal ganglia pathway forms a loop linking a vocal learning circuit with its dopaminergic input. *J Comp Neurol* **508**, 824-839, doi:10.1002/cne.21700 (2008).

4 Sutton, R. S. & Barto, A. G. *Reinforcement learning: an introduction*. (MIT Press, 1998).

5 Joel, D., Niv, Y. & Ruppin, E. Actor-critic models of the basal ganglia: new anatomical and computational perspectives. *Neural Netw* **15**, 535-547, doi:S0893-6080(02)00047-3 [pii] (2002).

6 Takahashi, Y., Schoenbaum, G. & Niv, Y. Silencing the critics: understanding the effects of cocaine sensitization on dorsolateral and ventral striatum in the context of an actor/critic model. *Front Neurosci* **2**, 86-99, doi:10.3389/neuro.01.014.2008 (2008).

7 Marler, P. Three models of song learning: evidence from behavior. *J Neurobiol* **33**, 501-516, doi:10.1002/(SICI)1097-4695(19971105)33:5<501::AID-NEU2>3.0.CO;2-8 [pii] (1997).

8 Gadagkar, V. *et al.* Dopamine neurons encode performance error in singing birds. *Science* **354**, 1278-1282, doi:10.1126/science.aah6837 (2016).

9 Hoffmann, L. A., Saravanan, V., Wood, A. N., He, L. & Sober, S. J. Dopaminergic Contributions to Vocal Learning. *J Neurosci* **36**, 2176-2189, doi:10.1523/JNEUROSCI.3883-15.2016
36/7/2176 [pii] (2016).

10 Xiao, L. *et al.* A Basal Ganglia Circuit Sufficient to Guide Birdsong Learning. *Neuron* **98**, 208-221 e205, doi:10.1016/j.neuron.2018.02.020 (2018).

11 Hisey, E., Kearney, M. G. & Mooney, R. A common neural circuit mechanism for internally guided and externally reinforced forms of motor learning. *Nature neuroscience*, 1 (2018).

12 Mandelblat-Cerf, Y., Las, L., Denisenko, N. & Fee, M. S. A role for descending auditory cortical projections in songbird vocal learning. *Elife* **3**, doi:10.7554/eLife.02152 (2014).

13 Gale, S. D. & Perkel, D. J. A basal ganglia pathway drives selective auditory responses in songbird dopaminergic neurons via disinhibition. *The Journal of neuroscience* **30**, 1027-1037, doi:10.1523/JNEUROSCI.3585-09.2010 (2010).

14 Person, A. L., Gale, S. D., Farries, M. A. & Perkel, D. J. Organization of the songbird basal ganglia, including area X. *J Comp Neurol* **508**, 840-866, doi:10.1002/cne.21699 (2008).

15 Andalman, A. S. & Fee, M. S. A basal ganglia-forebrain circuit in the songbird biases motor output to avoid vocal errors. *Proc Natl Acad Sci U S A* **106**, 12518-12523, doi:0903214106 [pii]
10.1073/pnas.0903214106 (2009).

16 Tumer, E. C. & Brainard, M. S. Performance variability enables adaptive plasticity of 'crystallized' adult birdsong. *Nature* **450**, 1240-1244, doi:nature06390 [pii]
10.1038/nature06390 (2007).

17 Murdoch, D., Chen, R. & Goldberg, J. H. Place preference and vocal learning rely on distinct reinforcers in songbirds. *Sci Rep* **8**, 6766, doi:10.1038/s41598-018-25112-5 (2018).

bioRxiv preprint doi: https://doi.org/10.1101/346841; this version posted June 14, 2018. The copyright holder for this preprint (which was not certified by peer review) is the author/funder. All rights reserved. No reuse allowed without permission.

18 Yu, A. C. & Margoliash, D. Temporal hierarchical control of singing in birds. *Science* **273**, 1871-1875 (1996).

19 Sober, S. J., Wohlgemuth, M. J. & Brainard, M. S. Central contributions to acoustic variation in birdsong. *J Neurosci* **28**, 10370-10379, doi:28/41/10370 [pii] 10.1523/JNEUROSCI.2448-08.2008 (2008).

20 Danish, H. H., Aronov, D. & Fee, M. S. Rhythmic syllable-related activity in a songbird motor thalamic nucleus necessary for learned vocalizations. *PloS one* **12**, e0169568 (2017).

21 Hamaguchi, K., Tanaka, M. & Mooney, R. A distributed recurrent network contributes to temporally precise vocalizations. *Neuron* **91**, 680-693 (2016).

22 Goldberg, J. H. & Fee, M. S. A cortical motor nucleus drives the basal ganglia-recipient thalamus in singing birds. *Nature Neuroscience* **15**, 620-627, doi:10.1038/nn.3047 nn.3047 [pii] (2012).

23 Haber, S. N., Fudge, J. L. & McFarland, N. R. Striatonigrostriatal pathways in primates form an ascending spiral from the shell to the dorsolateral striatum. *J Neurosci* **20**, 2369-2382 (2000).

24 Takahashi, Y. K., Langdon, A. J., Niv, Y. & Schoenbaum, G. Temporal Specificity of Reward Prediction Errors Signaled by Putative Dopamine Neurons in Rat VTA Depends on Ventral Striatum. *Neuron* **91**, 182-193, doi:10.1016/j.neuron.2016.05.015 S0896-6273(16)30175-1 [pii] (2016).

25 Surmeier, D. J., Ding, J., Day, M., Wang, Z. & Shen, W. D1 and D2 dopamine-receptor modulation of striatal glutamatergic signaling in striatal medium spiny neurons. *Trends in neurosciences* **30**, 228-235 (2007).

26 Fee, M. S. & Goldberg, J. H. A hypothesis for basal ganglia-dependent reinforcement learning in the songbird. *Neuroscience* **198**, 152-170, doi:S0306-4522(11)01175-4 [pii] 10.1016/j.neuroscience.2011.09.069 (2011).

27 Tchernichovski, O., Nottebohm, F., Ho, C. E., Pesaran, B. & Mitra, P. P. A procedure for an automated measurement of song similarity. *Anim Behav* **59**, 1167-1176, doi:10.1006/anbe.1999.1416 anbe.1999.1416 [pii] (2000).

28 Keller, G. B. & Hahnloser, R. H. Neural processing of auditory feedback during vocal practice in a songbird. *Nature* **457**, 187-190, doi:nature07467 [pii] 10.1038/nature07467 (2009).

29 Goldberg, J. H. & Fee, M. S. Singing-related neural activity distinguishes four classes of putative striatal neurons in the songbird basal ganglia. *Journal of Neurophysiology* **103**, 2002-2014, doi:10.1152/jn.01038.2009 01038.2009 [pii] (2010).

bioRxiv preprint doi: https://doi.org/10.1101/346841; this version posted June 14, 2018. The copyright holder for this preprint (which was not certified by peer review) is the author/funder. All rights reserved. No reuse allowed without permission.

Acknowledgements. Funding to JHG was provided by the NIH (grant # R01NS094667), the Pew Charitable Trust and the Klingenstein Neuroscience Foundations. Imaging data was acquired in the Cornell BRC-Imaging Facility using the shared, NIH-funded (S10RR025502) Zeiss LSM 710 Confocal. We thank Todd Roberts for providing virus, Joe Fetcho, Melissa Warden and Josh Dudman for comments, and Vikram Gadagkar, Aaron Andalman, and Dmitriy Aronov for analysis code.

Author Contributions. RC, PAP, ACR, TR, KM, AP, AF and JHG acquired data. RC, PAP, AP, KM and JHG analyzed data. RC and JHG wrote the manuscript.

Author Information. The authors declare no competing financial interests.

bioRxiv preprint doi: https://doi.org/10.1101/346841; this version posted June 14, 2018. The copyright holder for this preprint (which was not certified by peer review) is the author/funder. All rights reserved. No reuse allowed without permission.

Extended Data Fig. 1: AIV projects to VTA

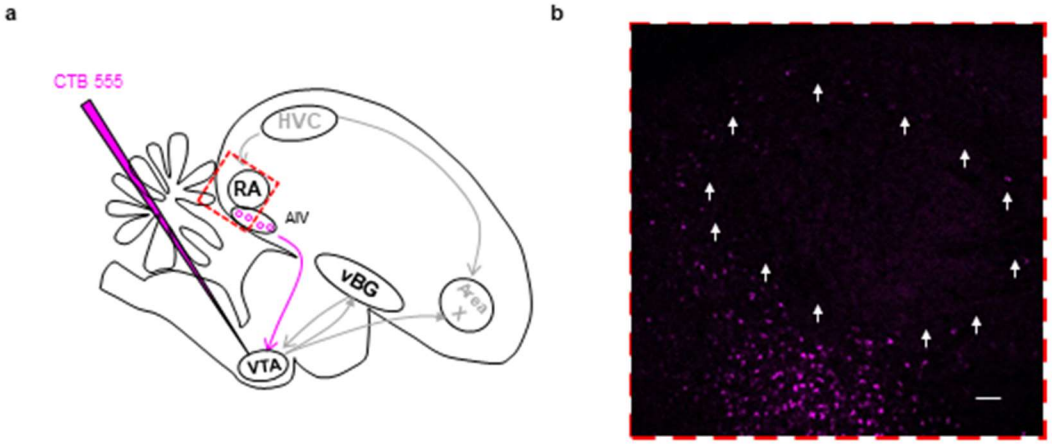

a, Schematic of tracing experiment. Injection of CTB-555 into VTA retrogradely labeled cell bodies in AIV, as previously reported[3,12]. **b,** Expanded view of red square from (**a**). VTA-projecting neurons are visible in AIV, which surrounds boundaries of RA, denoted by white arrows.

bioRxiv preprint doi: https://doi.org/10.1101/346841; this version posted June 14, 2018. The copyright holder for this preprint (which was not certified by peer review) is the author/funder. All rights reserved. No reuse allowed without permission.

Extended Data Fig. 2: Ventral basal ganglia projects to VTA

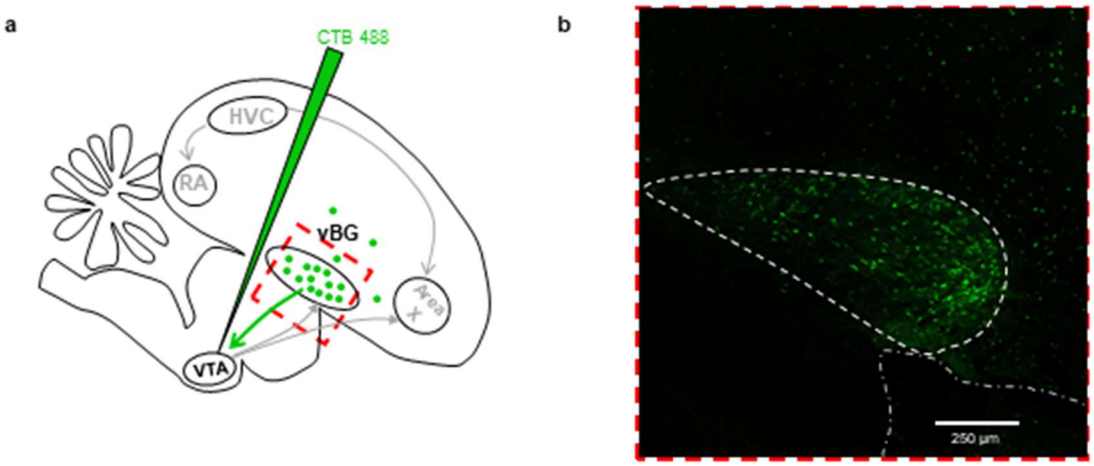

a, Schematic of tracing experiment. Injection of CTB-488 into VTA retrogradely labeled cell bodies in ventral basal ganglia, as previously reported[3]. **b,** Expanded view of red square from (**a**). VTA-projecting neurons are visible in VP, bounded by dashed white lines, and overlying striatum.

bioRxiv preprint doi: https://doi.org/10.1101/346841; this version posted June 14, 2018. The copyright holder for this preprint (which was not certified by peer review) is the author/funder. All rights reserved. No reuse allowed without permission.

Extended Data Fig. 3: vBG lesions impair song learning

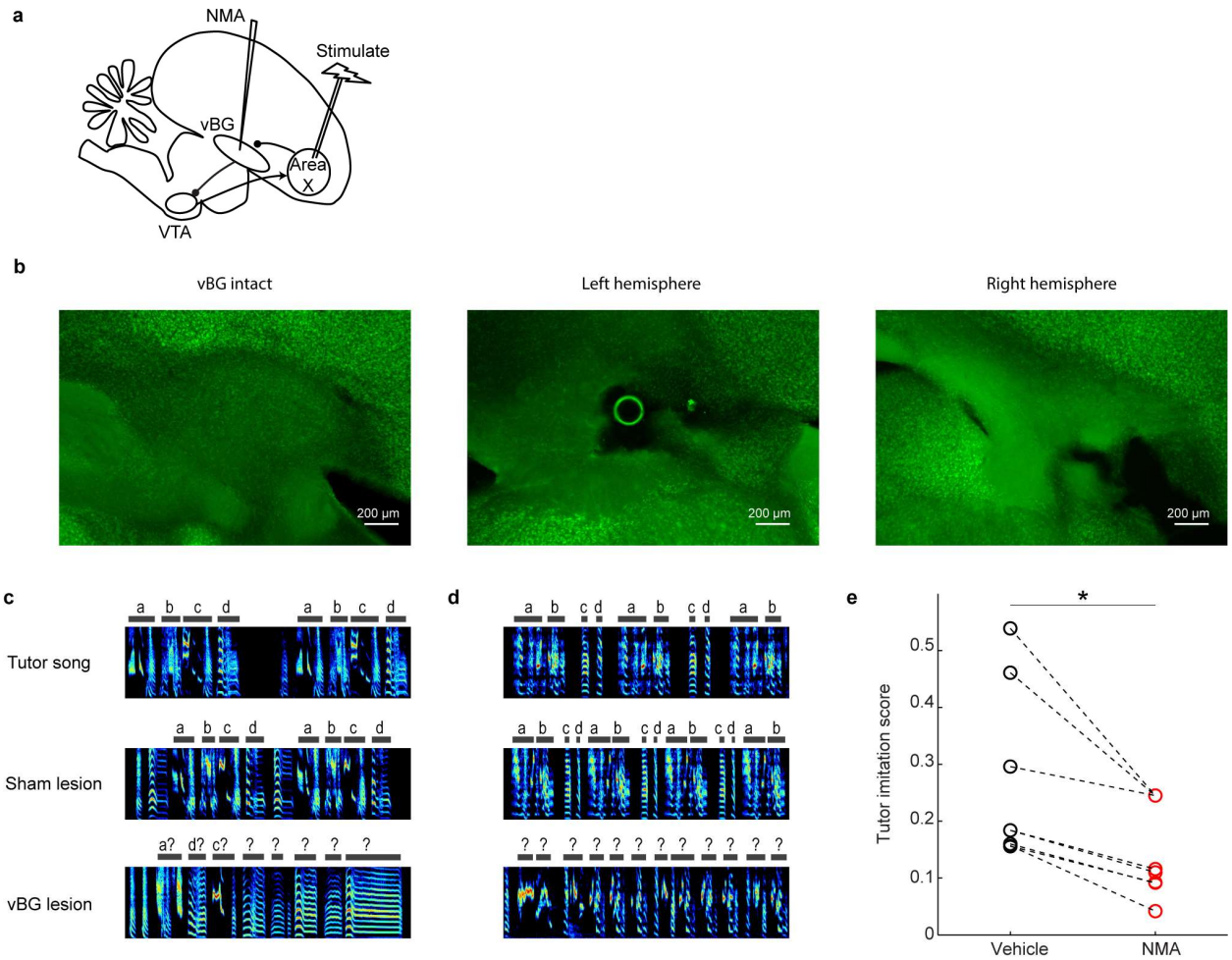

a, Schematic of lesion experiment. In juvenile birds (dph 39- 52) vehicle (n=7) or excitotoxin NMA (n=6) was injected bilaterally into vBG region, mapped intraoperatively by orthodromic response to Area X stimulation (Methods). **b,** Lesions were confirmed in neuronal nuclear stained (anti-NeuN) slices as extensive tissue damage and cell death. **c**, Tutor song (top), adult song of sham lesioned (middle), and vBG lesioned (bottom) siblings. **d**, same as (**c**) for another pair. **e**, Adult song of vBG lesioned birds had lower similarity to their tutor compared to controls (paired t test, p = 0.0416; rank-sum test between all controls and all lesioned birds, p = 0.014).

bioRxiv preprint doi: https://doi.org/10.1101/346841; this version posted June 14, 2018. The copyright holder for this preprint (which was not certified by peer review) is the author/funder. All rights reserved. No reuse allowed without permission.

Extended Data Fig. 4: Error response latencies and durations in vBG and VTA neurons

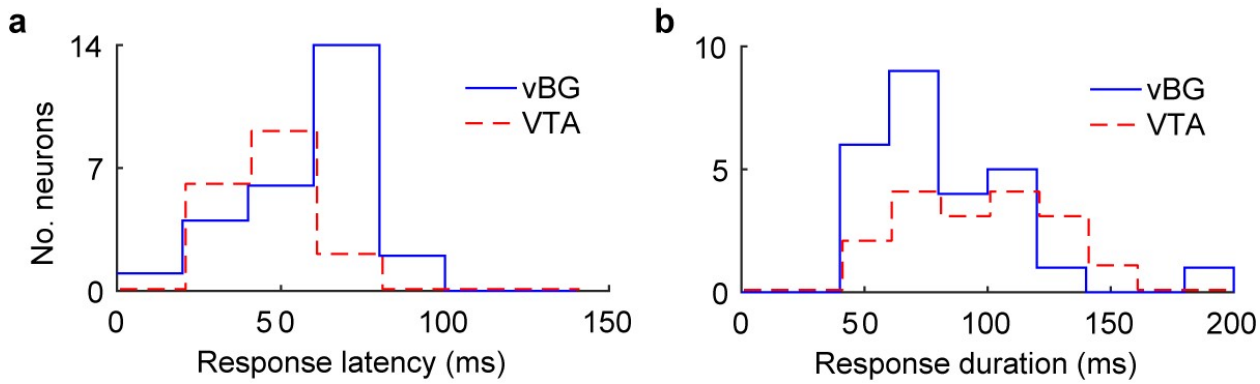

a, Histograms of response latency for all error responsive neurons. Blue: vBG neurons (n=29, range: 15 ms to 90 ms) Red: VTAerror neurons (n=17, range: 21 ms to 67 ms). **b**, Histogram of response duration for all error responsive neurons. Blue: vBG neurons (range: 45 ms to 210 ms) Red: VTA neurons (range: 58 ms to 148 ms). VTA data taken from a previous study[8]

bioRxiv preprint doi: https://doi.org/10.1101/346841; this version posted June 14, 2018. The copyright holder for this preprint (which was not certified by peer review) is the author/funder. All rights reserved. No reuse allowed without permission.

Extended Data Fig. 5: Animal movement was not affected by DAF during singing

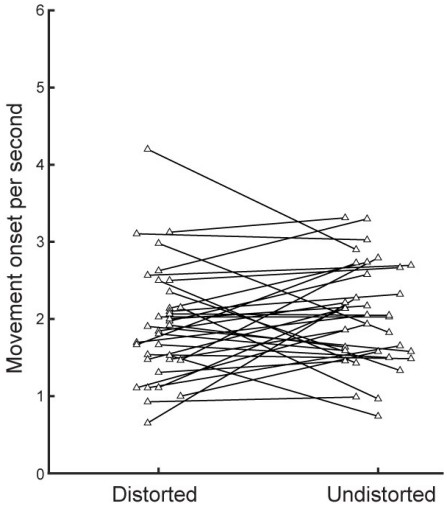

Analysis of DAF-related movement responses across all birds. Each line represents data from one bird with average rate of movement onsets in 150 ms following distorted and undistorted syllables. There was no difference in movement between distorted and undistorted motifs ($p > 0.05$ in 35/35 birds, WRS test.)

bioRxiv preprint doi: https://doi.org/10.1101/346841; this version posted June 14, 2018. The copyright holder for this preprint (which was not certified by peer review) is the author/funder. All rights reserved. No reuse allowed without permission.

Extended Data Fig. 6: vBG responses during active singing and passive listening to bird's own song.

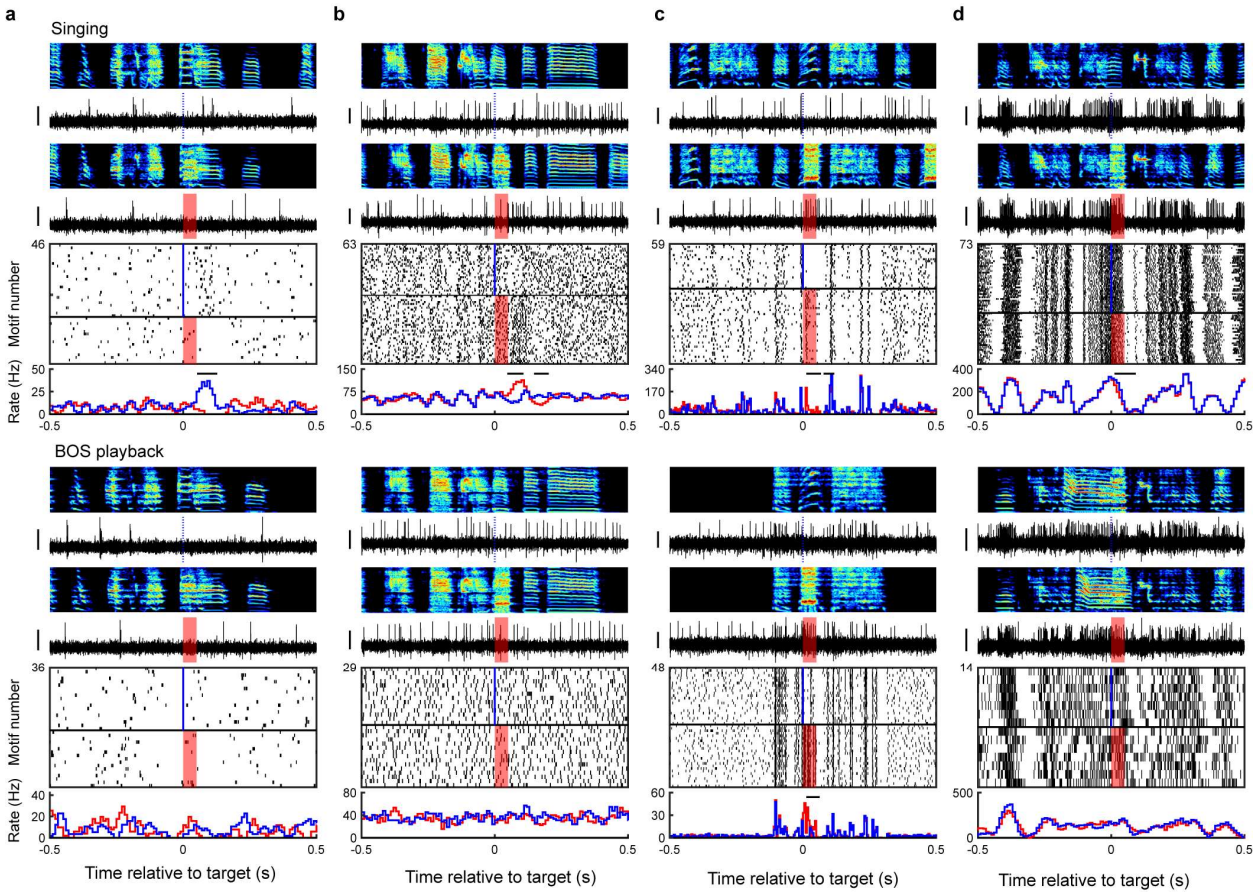

a-d, Examples of four neurons recorded during active singing, top row, and during passive playback of bird's own song (BOS), bottom row. Data plotted as in Fig. 2b for all neurons in both conditions. Shown are examples of neurons that exhibited error responses only during singing (**a-b**) and the only two putatively auditory neurons recorded in the dataset, which exhibited strong auditory responses to playback of BOS. Neuron in (**b**) is the vBGvta neuron from main Fig. 4e.

bioRxiv preprint doi: https://doi.org/10.1101/346841; this version posted June 14, 2018. The copyright holder for this preprint (which was not certified by peer review) is the author/funder. All rights reserved. No reuse allowed without permission.

Extended Data Fig. 7: Examples of singing- and error-related representations in vBG.

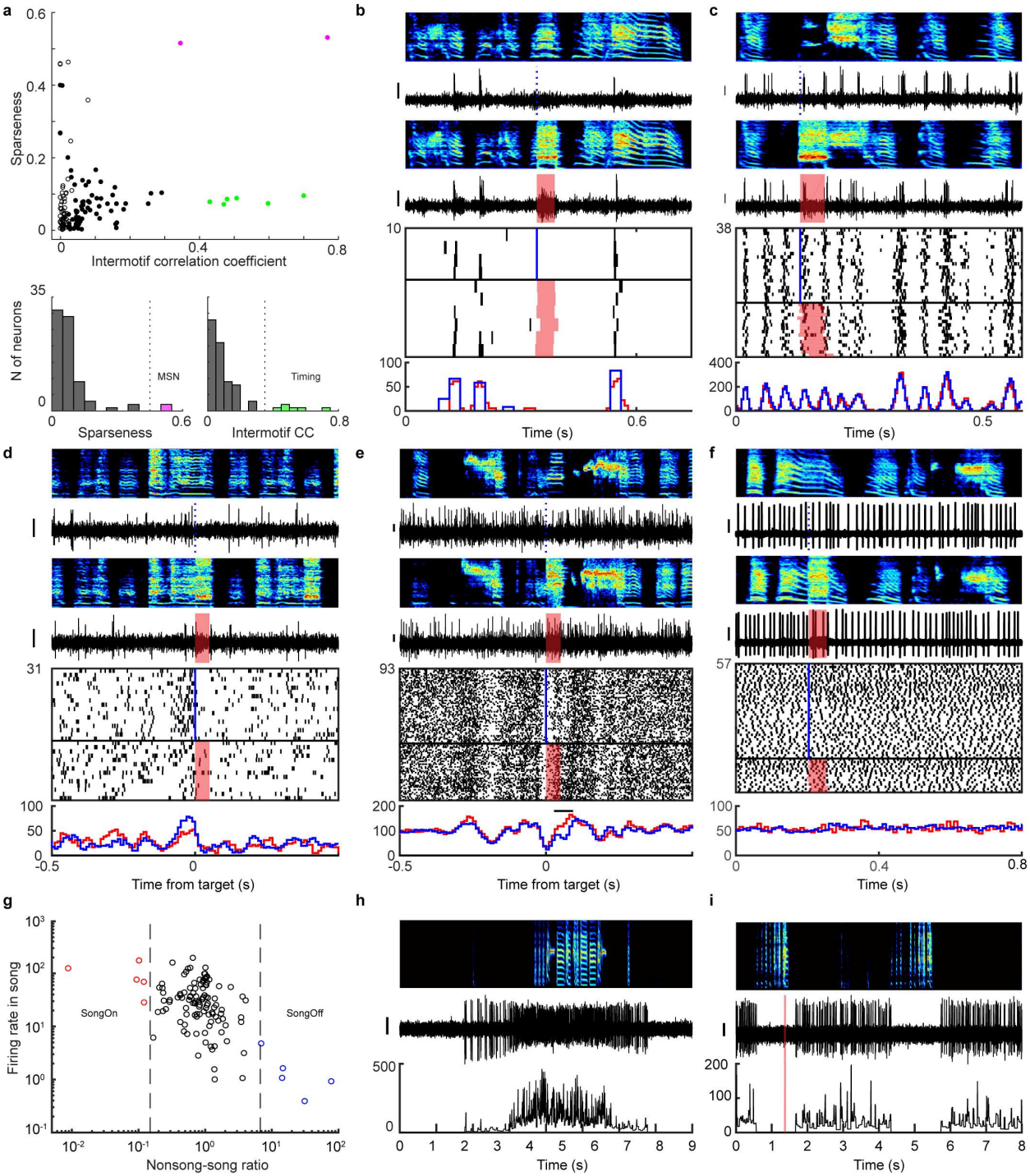

a, Sparseness and intermotif correlation coefficient (ICC) distinguished two classes of time-locked vBG neurons. **b**, MSN-like vBG neuron with sparse bursts time-locked to song motif. **c**, vBG neuron with stereotyped high frequency bursts that tile the song motif. **d**, Pre-target bursting neuron with high firing rate immediately before song target. **e**, Pre-target pause neuron that was also error-activated. **f**, vBG neuron unrelated to singing. **g**, The ratio between mean

bioRxiv preprint doi: https://doi.org/10.1101/346841; this version posted June 14, 2018. The copyright holder for this preprint (which was not certified by peer review) is the author/funder. All rights reserved. No reuse allowed without permission.

firing rates outside and inside of singing identified vBG neurons gated by singing state. **h**, Example song-activated neuron which fired at high rate during singing, but silent outside song. **i**, Example song-suppressed neuron abruptly stopped firing during singing.

bioRxiv preprint doi: https://doi.org/10.1101/346841; this version posted June 14, 2018. The copyright holder for this preprint (which was not certified by peer review) is the author/funder. All rights reserved. No reuse allowed without permission.

Extended Data Fig. 8: Diverse vBG cell types were spatially intermingled.

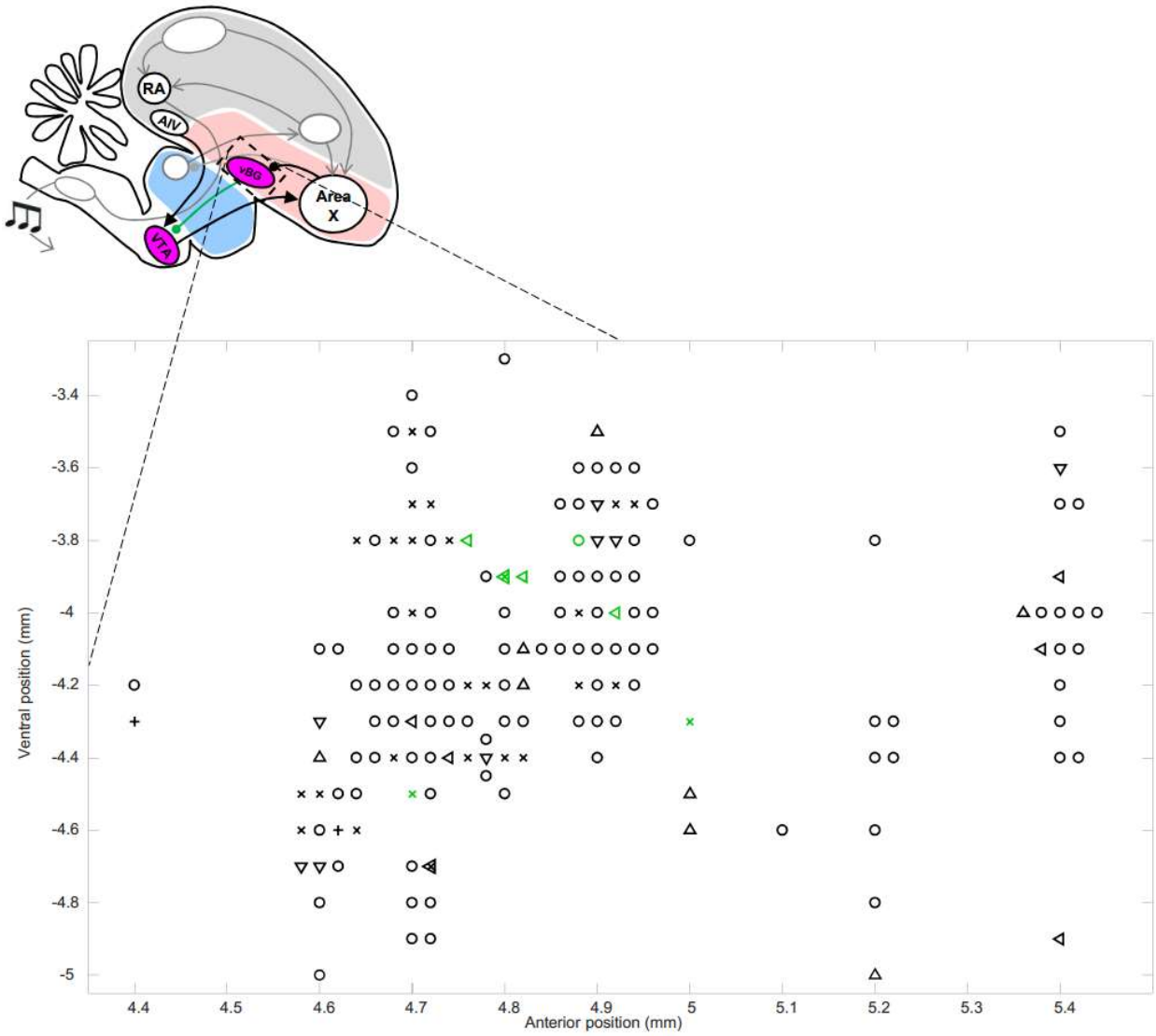

Top, schematic of bird brain. Bottom, expanded view of the vBG region recorded, with the estimated position of each recorded neuron in the dataset. Mediolateral coordinates of 1.1 - 1.5 mm from midline are collapsed in this image. Cell type symbols: VTA-projecting (green), error responsive (x), MSN and burst-tiling (△), song-activated or song-suppressed (▽), pre-target burst or pause (◁), auditory (+), other (o).

bioRxiv preprint doi: https://doi.org/10.1101/346841; this version posted June 14, 2018. The copyright holder for this preprint (which was not certified by peer review) is the author/funder. All rights reserved. No reuse allowed without permission.

Extended Data Fig. 9: RA projects to vBG

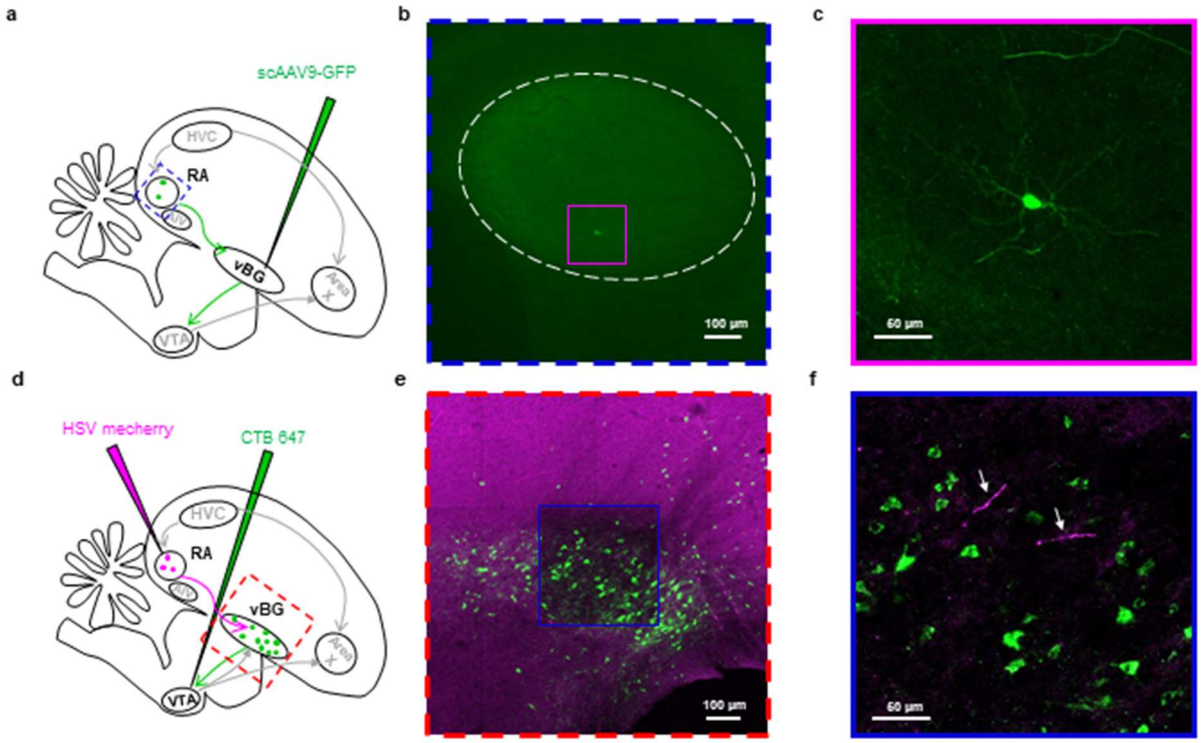

Combined anterograde and retrograde strategies were used to confirm RA projection to vBG. **a,** Sparse retrograde virus (scAAV9-GFP) was injected into vBG. **b,** Fluorescently labeled RA neuron, centered in pink box (dashed white lines denote RA boundaries). **c,** Expanded view of the pink box from (**b**) revealing GFP-expressing vBG-projecting RA neuron. **d,** In anterograde strategy, anterograde virus (HSV-mCherry) was injected into RA and CTB-647 was injected into VTA. **e,** Photomicrograph of vBG region, with VTA-projecting neurons clearly visible (green). **f,** Exapnded view from blue box in (**e**), revealing proximity of RA axons (purple) to VTA-projecting neurons in vBG.

bioRxiv preprint doi: https://doi.org/10.1101/346841; this version posted June 14, 2018. The copyright holder for this preprint (which was not certified by peer review) is the author/funder. All rights reserved. No reuse allowed without permission.

Extended Data Fig. 10. Uva, AIV, DLM, Ov and VTAx project to vBG.

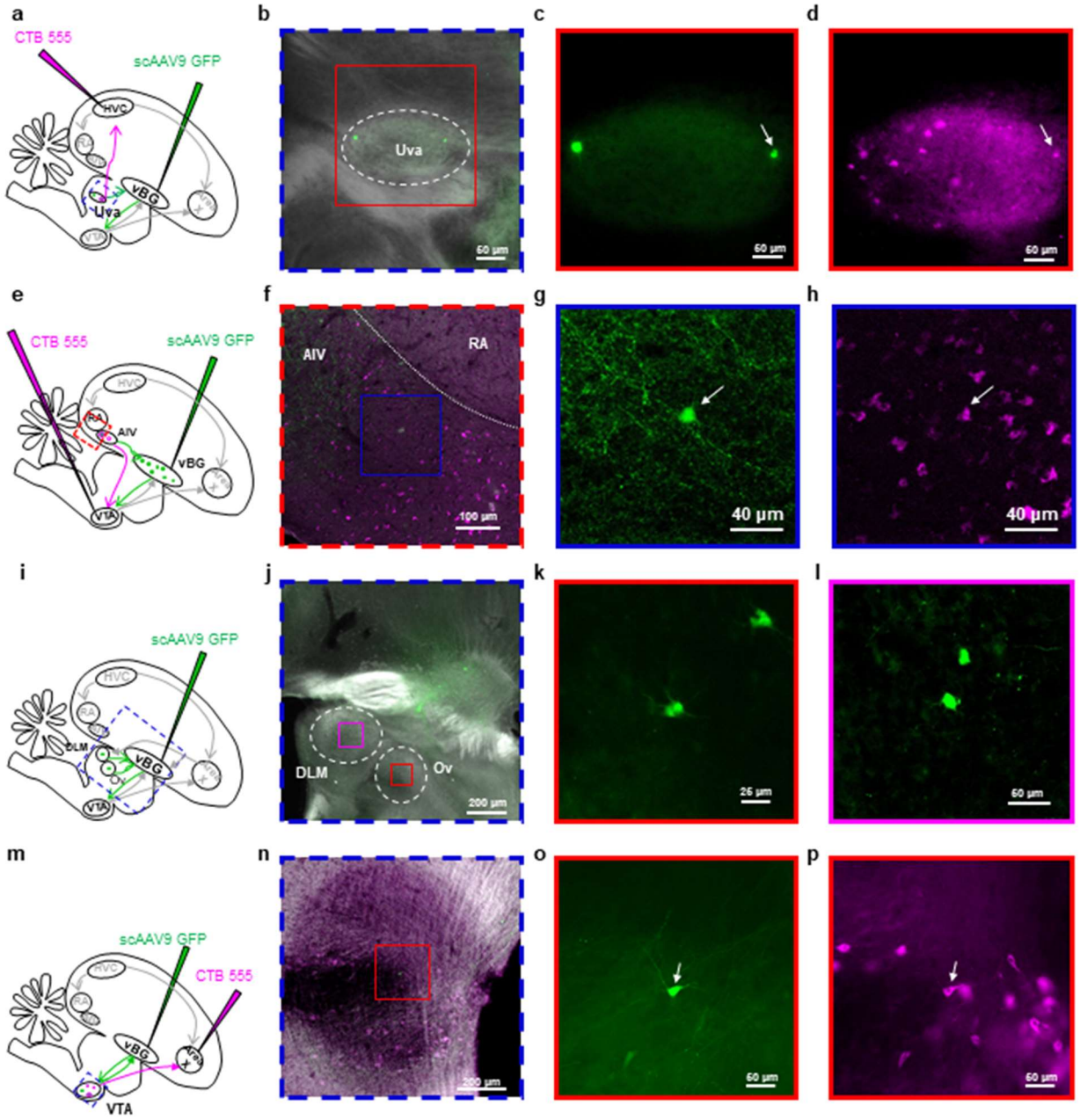

To label vBG-projecting neurons, sparse retrograde scAAV9 virus was injected into vBG (**a**,**e**,**i**,**m**). **A**-**d**, HVC-projecting nucleus Uvaeformis (Uva) thalamic neurons project to vBG. CTB-555 was injected into HVC (**a**). Retrogradely labeled vBG-projecting Uva neuron (arrow, **c**) was colabeled with HVC-projecting Uva neuron (arrow, **d**). **e**-**h**, VTA-projecting AIV neurons also project to vBG. CTB-555 was injected into VTA (**e**). Retrogradely labeled vBG-projecting AIV neuron (arrow, **g**) is colabeled with VTA-projecting AIV neuron (arrow, **h**). **i**-**l**, Area X recipient thalamus DLM and primary auditory thalamus Ovoidalis (Ov) project to vBG.

bioRxiv preprint doi: https://doi.org/10.1101/346841; this version posted June 14, 2018. The copyright holder for this preprint (which was not certified by peer review) is the author/funder. All rights reserved. No reuse allowed without permission.

Retrogradely labeled DLM neurons (**k**) and Ov (**l**). **m**-**p**, Area X-projecting VTA dopamine neurons (VTAx) send collaterals to vBG. CTB-555 was injected into Area X (**m**). Retrogradely labeled vBG-projecting VTA neuron (arrow, **o**) was colabeled with X-projecting VTA neuron (arrow, **p**).